



RESEARCH ARTICLE

Modelling the effect of experimental conditions that influence rundown of L-type calcium current

[version 1; peer review: awaiting peer review]

Aditi Agrawal ^{1,2}, Michael Clerx ², Ken Wang³, Liudmila Polonchuk³, Gary R. Mirams ², David J. Gavaghan ¹

¹Computer Science, University of Oxford, Oxford, England, OX1 3QD, UK

²University of Nottingham School of Mathematical Sciences, Nottingham, England, NG7 2RD, UK

³Pharma Research and Early Development, F. Hoffman-LaRoche, Basel, CH-4070, Switzerland

V1 First published: 20 Mar 2025, 10:157
<https://doi.org/10.12688/wellcomeopenres.23558.1>

Latest published: 20 Mar 2025, 10:157
<https://doi.org/10.12688/wellcomeopenres.23558.1>

Open Peer Review

Approval Status AWAITING PEER REVIEW

Any reports and responses or comments on the article can be found at the end of the article.

Abstract

Background

L-type calcium channels (LCCs) are macro-molecular complexes that conduct I_{CaL} and are involved in several critical functions in cardiac, skeletal, neuronal, smooth muscle, and endocrine cells. In common with other ionic channels they can be studied by isolating and overexpressing in a cell line, and the current through them can be measured using patch-clamp experiments. However, LCC current recordings are known to be contaminated with attenuation of current, known as 'rundown'. Previous work has shown that increased accumulation of intracellular calcium is likely associated with increased rundown.

Methods

We built a mathematical model of I_{CaL} conducted by LCCs overexpressed in CHO cells and systematically investigated the qualitative impact of both user-defined as well as experimental parameters within the typical patch-clamp setup on I_{CaL} rundown.

Results

Simulations show that calcium-dependent inactivation (CDI) of LCCs modestly contributes towards experimentally observed rundown. The underlying reason for the experimental rundown due to CDI (RCDI) was found to be the non-instantaneous diffusion and reactions of

calcium and the calcium-chelating buffer inside the cell. In this study we show that RCDI occurs when the buffer does not have sufficient time to diffuse into the cell; both after patching before the LCCs are activated, and also during the experiment progression. This finding was validated by showing that rundown due to accumulation of Ca^{2+} can be reduced by increasing the concentration of the calcium-chelating buffer in the intracellular solution.

Conclusions

To minimise rundown due to CDI, we suggest optimising independent experimental parameters such as buffer concentration and the time scales for diffusion to enable buffer equilibration into the cell. Additionally, we suggest that use of large cells should be avoided since they are more prone to RCDI.

Plain language summary

Cardiac electrical activity co-ordinates the heartbeat, and happens as a result of ion currents flowing in and out of cardiac muscle cells. One of these currents is known as the “Long-lasting” or “L-type” calcium current and experimental recordings of this current are particularly prone to a phenomenon called “rundown” in which the magnitude of the current reduces over time. In a previous article we presented experimental findings on rundown in different experimental conditions. One of the most important experimental factors is the presence of calcium buffers, which bind with free calcium ions to reduce their concentration. This is intended to reduce ‘knock-on effects’ associated with high calcium concentrations within the cell, which could be unwanted or even toxic. One such effect is increased inactivation of the L-type channels as they are sensitive to the calcium concentration inside the cell. Here we provide a mathematical modelling approach to show the importance of buffering in determining rundown, and how the effects depend upon the size of the cell, and the amount of time that is allowed for the buffer to diffuse into the cell before and during the experiments.

Keywords

L-type calcium current, rundown, diffusion, patch-clamp, voltage-clamp, ionic channels, electrophysiology

Corresponding author: Gary R. Mirams (gary.mirams@nottingham.ac.uk)

Author roles: **Agrawal A:** Conceptualization, Data Curation, Formal Analysis, Investigation, Methodology, Software, Visualization, Writing – Original Draft Preparation; **Clerx M:** Conceptualization, Formal Analysis, Methodology, Supervision, Writing – Review & Editing; **Wang K:** Conceptualization, Formal Analysis, Methodology, Supervision, Writing – Review & Editing; **Polonchuk L:** Conceptualization, Funding Acquisition, Investigation, Methodology, Project Administration, Resources, Supervision, Writing – Review & Editing; **Mirams GR:** Conceptualization, Funding Acquisition, Methodology, Project Administration, Supervision, Writing – Review & Editing; **Gavaghan DJ:** Conceptualization, Data Curation, Formal Analysis, Investigation, Methodology, Project Administration, Supervision, Validation, Writing – Original Draft Preparation, Writing – Review & Editing

Competing interests: K.W. & L.P. are employees and shareholders of L.Hoffman-La Roche.

Grant information: This work was supported by Wellcome [212203, <https://doi.org/10.35802/212203>]; the UK Engineering and Physical Sciences Research Council [EP/L016044/1, EP/S024093/1]; the Biotechnology and Biological Sciences Research Council [BB/P010008/1]. A.A. acknowledges EPSRC and F. Hoffmann-La Roche Ltd. for studentship support via the Centre for Doctoral Training in Systems Approaches to Biomedical Science. D.J.G. acknowledges support from the EPSRC Centres for Doctoral Training Programme. G.R.M., M.C. and D.J.G. acknowledge support from a BBSRC project grant. G.R.M. and M.C. acknowledge support from the Wellcome Trust via a Senior Research Fellowship to G.R.M.

The funders had no role in study design, data collection and analysis, decision to publish, or preparation of the manuscript.

Copyright: © 2025 Agrawal A *et al.* This is an open access article distributed under the terms of the [Creative Commons Attribution License](#), which permits unrestricted use, distribution, and reproduction in any medium, provided the original work is properly cited.

How to cite this article: Agrawal A, Clerx M, Wang K *et al.* **Modelling the effect of experimental conditions that influence rundown of L-type calcium current [version 1; peer review: awaiting peer review]** Wellcome Open Research 2025, 10:157 <https://doi.org/10.12688/wellcomeopenres.23558.1>

First published: 20 Mar 2025, 10:157 <https://doi.org/10.12688/wellcomeopenres.23558.1>

Introduction

The *L-type calcium current* (I_{CaL}), conducted by the L-type calcium channels (LCCs), is responsible for maintenance of the ‘plateau phase’ of the cardiac action potential and the initiation of excitation-contraction coupling in the heart. Brugada and Timothy syndromes are examples of long and short QT disorders occurring congenitally where LCC is mutated¹. Given the importance of I_{CaL} , modulations in its function that occur congenitally or via unintended pharmaceutical interactions can expose a patient to increased risk of sudden cardiac death.

The principal proteins forming many ionic channels, including LCCs, can be overexpressed in a candidate cell line and the current through them can subsequently be measured using the patch-clamp technique². However, patch-clamp recordings of I_{CaL} are known to be affected by attenuation of the current magnitude with time, known as *rundown*. Several reasons for rundown have been proposed, including time-dependent phenomena such as loss of phosphorylating agents (e.g. ATP) or loss of LCCs from the membrane^{3,4}. Some works have also indicated that calcium accumulation inside the cell contributes towards rundown of I_{CaL} ^{5,6}. Previous work from our group has also shown that I_{CaL} rundown is stronger at experimental conditions that are expected to promote the accumulation of calcium inside the cells, thus suggesting that calcium-dependent inactivation (CDI) is at least in part responsible for rundown⁷. These rundown promoting conditions included: high frequency of the voltage steps at which LCCs open; block of the sodium-calcium exchanger — preventing extrusion of sub-membrane calcium; and higher temperature resulting in larger I_{CaL} influx. We also showed that the rundown-versus-time curve took one of three predominant qualitative shapes including linear, saturating, and ‘inverse’ patterns. **Figure 1** shows an example of the rundown of I_{CaL} recorded from the previous study.

In this study, we developed a mechanistic reaction-diffusion model to simulate calcium-dependent inactivation (CDI) and qualitatively reproduce experimentally observed rundown patterns of I_{CaL} in CHO cells overexpressing $Ca_v1.2$ observed in previous work⁷. Modelled on an automated (planar patch)-clamp chip, we assume the cells form an approximately hemispherical shape (**Figure 2**). Prior to the application of a voltage-clamp protocol, intracellular calcium-chelating buffer BAPTA (denoted ‘B’) diffused throughout the cell over a duration ‘ t_0 ’ (**Figure 2** (left)). This time period is no larger than the time between cells being added to the plate and initiation of the voltage clamp protocol, which is identical across a whole 384-well plate, but can be shorter in a cell-specific way (see Methods for further details). The voltage-clamp protocol included repeated steps to 0mV (with time t_{hold} between successive sweeps) which induces LCC opening, introduces Ca^{2+} into the cell, and triggers CDI. Incoming Ca^{2+} reacts with free buffer, forming ‘CaB’ and creating a radial concentration gradient (**Figure 2**, centre). The model considered chemical reaction and diffusion of Ca^{2+} , B and CaB due to I_{CaL} (**Figure 2**, right) and the resulting impact on CDI, and how CDI changes for successive voltage-steps (rundown due to CDI, termed ‘RCDI’). We used the model to explore the influence of specific parameters on RCDI: 1) experimental parameters which are difficult to control or measure precisely (channel permeability

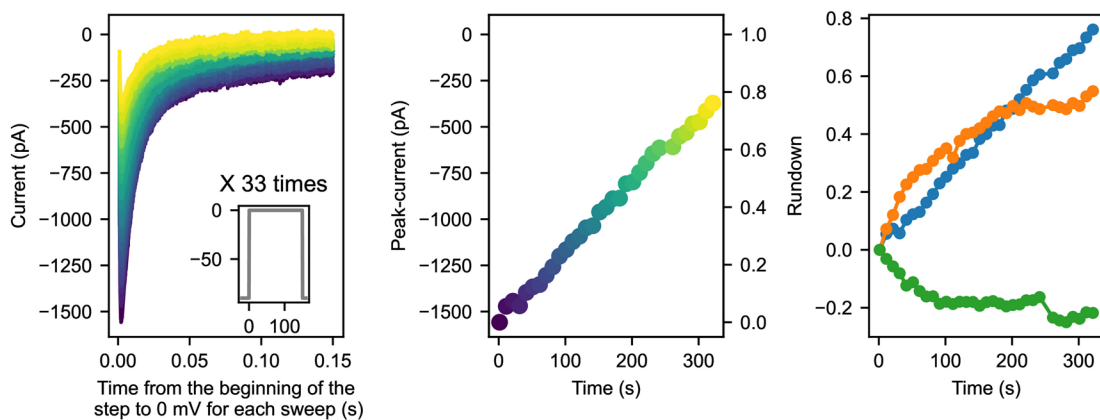


Figure 1. Illustration of rundown of L-type calcium current (I_{CaL}) from previous patch-clamp experiments⁷. Left: I_{CaL} recorded at successive channel opening steps overlaid with first and last step to 0mV shown in indigo and yellow recordings respectively. Inset: voltage-clamp protocol during which current is recorded, interspersed by a holding potential at -90 mV for 10 s. Centre: peak I_{CaL} recorded at different times on the left axis, and rundown at each sweep on the right axis. Right: examples of three common types of rundown-versus-time curves observed experimentally.

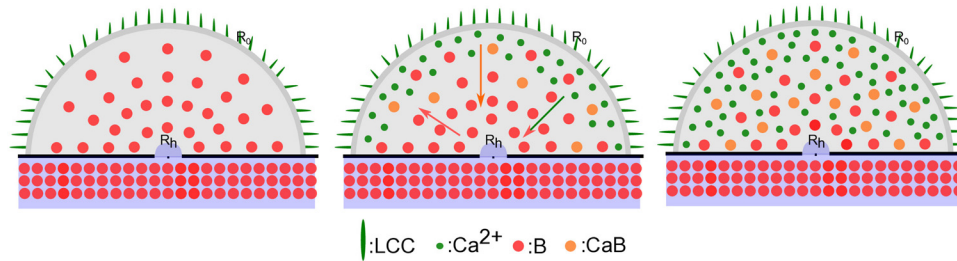


Figure 2. Schematic depicting the sequence of events described in text. Left: Cell placed on a seal chip before the voltage-clamp is applied and after buffer (B) has equilibrated into the cell. Centre: Ca^{2+} enters the cell via the LCCs and reacts with B to form CaB, creating a concentration gradient for all three chemical species. Right: Ca^{2+} , B, and CaB have diffused into the cell according to the concentration gradient, and a pseudo-steady-state profile over time can be set up (periodic as the voltage clamp causes periodic Ca^{2+} influx), but it is not spatially homogenous due to the boundary conditions — there is more calcium near the membrane and more buffer near the patch hole.

(\bar{P}_{Ca}), cell size (R_0 , t_0); and 2) user-defined parameters (t_{hold} and maximum B concentration (B_{max})). Both experimental and user-defined parameters were estimated or set to match the expected experimental conditions in Agrawal *et al.*⁷.

We will use the model to establish qualitative trends of rundown and show that RCDI occurs when there is a change across sweeps in the availability of the calcium-chelating buffer near the LCCs. This creates an accumulation or depletion in sub-membrane calcium concentration, $[\text{Ca}^{2+}]_s$, per sweep leading to saturating or inverse patterns of the rundown-versus-time curve, thus explaining two of the three patterns observed previously. We find that within the range of the experimental variables in Agrawal *et al.*⁷, noticeable RCDI only occurs for large cells and not for the average-sized cell, suggesting that CDI only plays a modest role in contributing towards total rundown observed experimentally. We then use the model to establish that RCDI can be determined by the interplay of three different time constants that affect [B] inside the cell — t_0 , t_{hold} and t_{diff} (a function of R_0 indicating the time required for B to *diffuse* across the cell). The role of buffer dynamics in causing RCDI is further confirmed by showing that increasing B_{max} reduces run-down. The study shows that RCDI can be minimised by working with smaller cells because they allow buffer to better equilibrate within the cell both before and during a voltage-clamp experiment.

Methods

Data availability

The results presented in this study were generated using Python version 3.10.11 and all data, code, and supporting material are available at <https://github.com/CardiacModelling/L-type-Ca-rundown-modelling>. A permanently archived version is available on Zenodo at <https://doi.org/10.5281/zenodo.14186292>.

Some extended plots and data that support this study but are not essential to comprehend the results can be viewed at <https://github.com/CardiacModelling/L-type-Ca-rundown-modelling/blob/main/ExtendedData.ipynb>.

Reaction-diffusion model formulation

Ca^{2+} is brought into the cell by I_{CaL} , which initiates a cascade of events involving diffusion and chemical reaction as shown in Figure 2. In this section, we describe the equations that account for these processes.

The chemical reaction of calcium and the free buffer is considered to be a mass-action reaction, qualitatively illustrated by:



where CaB is the calcium-buffer complex, and k_{on} and k_{off} are the rates of forward and backward reactions respectively. Note that BAPTA actually binds two calcium ions in separate reactions, but we use Equation (1) for simplicity here as this feature is not expected to alter the trends we are investigating. The three chemical species (Ca^{2+} , B, and CaB) simultaneously diffuse according to their chemical gradient as well as reacting as per

Equation (1). By accounting for both the diffusion and the mass-action reaction of these chemical species, the rate of change of each species can be written using a partial differential equation (PDE) in spherical polar coordinates as:

$$\frac{\partial[B]}{\partial t} = \overbrace{\frac{D_B}{r^2} \frac{\partial}{\partial r} \left(r^2 \frac{\partial[B]}{\partial r} \right)}^{\text{diffusion}} - \overbrace{(k_{on} \cdot [Ca^{2+}][B] - k_{off} \cdot [CaB])}^{\text{chemical reaction}} \quad (2)$$

$$\frac{\partial[Ca^{2+}]}{\partial t} = \frac{D_{Ca}}{r^2} \frac{\partial}{\partial r} \left(r^2 \frac{\partial[Ca^{2+}]}{\partial r} \right) - (k_{on} \cdot [Ca^{2+}][B] - k_{off} \cdot [CaB]), \quad (3)$$

$$\frac{\partial[CaB]}{\partial t} = \frac{D_B}{r^2} \frac{\partial}{\partial r} \left(r^2 \frac{\partial[CaB]}{\partial r} \right) + (k_{on} \cdot [Ca^{2+}][B] - k_{off} \cdot [CaB]). \quad (4)$$

Here, D_{Ca} and D_B are the diffusion coefficients of calcium and buffer respectively. The diffusion coefficient of the CaB complex was assumed to be the same as that of the buffer because of the much higher molecular weight of the buffer (BAPTA, ~760 Da) compared to Ca^{2+} (~40 Da). We work with time relative to the beginning of the voltage clamp application, such that $t = 0$ is at the end of the time period t_0 . The initial and boundary conditions at $r = R_0$ and $r = R_h$ for each of these chemical quantities are then given as:

$$\begin{aligned} r = R_h, \quad [B] = B_{\max}, \quad [Ca^{2+}] = 0, \quad [CaB] = 0; \\ r = R_0, \quad \frac{\partial[B]}{\partial r} = 0, \quad \frac{\partial[Ca^{2+}]}{\partial r} = \frac{-I_{Ca}^{Ca}}{2FAD_{Ca}}, \quad \frac{\partial[CaB]}{\partial r} = 0; \\ t = 0, \quad [B] = f(r, t_0), \quad [Ca^{2+}] = 0, \quad [CaB] = 0; \end{aligned} \quad (5)$$

Here, A is the surface area of the cell and F is Faraday's constant. The initial condition for the buffer is a function of both the radial distance from the centre (r) and the time the buffer has to diffuse into the cell before the LCCs open (t_0). This is given by $f(r, t_0)$ and can be easily calculated for each r given R_0 and t_0 using the analytical solution for diffusion of buffer in this geometry given by Agrawal *et al.*⁸. As $t_0 \rightarrow \infty$, B approaches spatial uniformity (B_{\max} throughout) at $t = 0$, in which case CaB would simply follow $[CaB] = B_{\max} - [B]$ rather than its own PDE. However, in practice, complete equilibration of the free buffer into the cell only occurs for small cells. The equations governing I_{CaL} are given in the next section and are a function of membrane voltage (V_m), local $[Ca^{2+}]$ near the LCCs ($[Ca^{2+}]_s$), and time.

Model of the L-type calcium current

Although a small amount of other ions can move through LCCs, I_{CaL} is primarily carried by Ca^{2+9} :

$$I_{CaL} \approx I_{CaL}^{Ca} = \bar{P}_{Ca} \cdot \delta_{GHK} \cdot O, \quad (6)$$

where, O is the open probability of a single channel and \bar{P}_{Ca} is the maximum permeability which is a function of the channel density in a membrane. δ_{GHK} is the electrochemical force driving the ionic movement, which is calculated using the GHK flux equation:

$$\delta_{GHK} = V_m \frac{z^2 F^2}{R_g T} \left(\frac{\gamma_{in} [Ca]_s - \gamma_{out} [Ca]_{out} \exp(-zV_m F / R_g T)}{1 - \exp(-zV_m F / R_g T)} \right), \quad (7)$$

where z is the valance of Ca^{2+} , V_m is the membrane voltage, T is the temperature, R_g is the universal gas constant, $[Ca]_{out}$ is the extracellular concentration, $[Ca]_s$ is the submembrane concentration, the activity coefficient γ accounts for the deviation of the ionic species from ideal behaviour in the intracellular and extracellular solutions¹⁰.

For simplicity, in this study, we adopted O from the I_{CaL} model proposed by Zeng *et al.*¹¹ because it uses an instantaneous gate given by Hill's equation to describe the CDI kinetics of LCCs (gate f_{Ca}). We expect the results of this study to be unaffected by the choice of this gate because CDI is a fast process, occurring over 20 to 100 ms compared to tens, or even hundreds of seconds required for diffusion¹²⁻¹⁴. The overall kinetics is given by simple gating (see **Type C1** in Agrawal *et al.*⁹) in which the voltage-dependent kinetics are the product of two Hodgkin-Huxley style gating variables¹⁵ representing activation (gate d) and inactivation (gate f). Therefore, the overall gating structure of the model is $O = d \cdot f \cdot f_{Ca}$, where:

$$\frac{dd}{dt} = \frac{d_{\infty} - d}{\tau_d}, \quad \frac{df}{dt} = \frac{f_{\infty} - f}{\tau_f}, \quad f_{Ca} = \frac{1}{1 + [Ca^{2+}]_s / K_{IC50}}. \quad (8)$$

Here, d_{∞} , f_{∞} , τ_d , and τ_f are functions of V_m ; and K_{IC50} is the $[Ca^{2+}]_s$ at which the f_{Ca} becomes half. The original parameters of the model by Zeng *et al.*¹¹ were retained except for the activity coefficients which were modified to be computed using the Davies equation¹⁶.

For the sake of simplicity, I_{CaL} was considered as the only source of Ca^{2+} inside the cell and contribution by other currents such as leak current (due to imperfect seal) was ignored.

Voltage-clamp protocol

Ca^{2+} enters the cell via I_{CaL} thus initiating its chemical reaction with B and diffusion towards the centre of the cell. I_{CaL} opens and conducts current in response to the changes in the membrane voltage (V_m), which is clamped according to a voltage-clamp protocol.

In this study, the protocol consists of a holding potential of -90 mV with repeated pulses to 0 mV for 120 ms interspersed with a holding potential for a duration set to either 10 , 20 , or 40 s (t_{hold}) as shown in [Figure 3](#). The step to 0 mV was chosen because the LCCs are known to open and conduct I_{CaL} at this voltage⁹.

Experimental range and default values

In this section, we explain how the parameters for the model were determined from the experimental design and results of the previous patch-clamp experiment.

In this study, independent model parameters are either user-defined or determined through the experimental setup. For instance, the parameter t_{hold} has three distinct values, as detailed in the previous section. B_{max} is assigned a value of 10 mM to align with the BAPTA concentration used in patch-clamp experiments. Additionally, the inner boundary radius (R_h) is derived by projecting the surface area of a patch hole with radius $1 \mu\text{m}$ onto a hemisphere, resulting in R_h being $1/\sqrt{2} \mu\text{m}$ (see [Figure 2](#)). This projection ensures that the planar patch surface

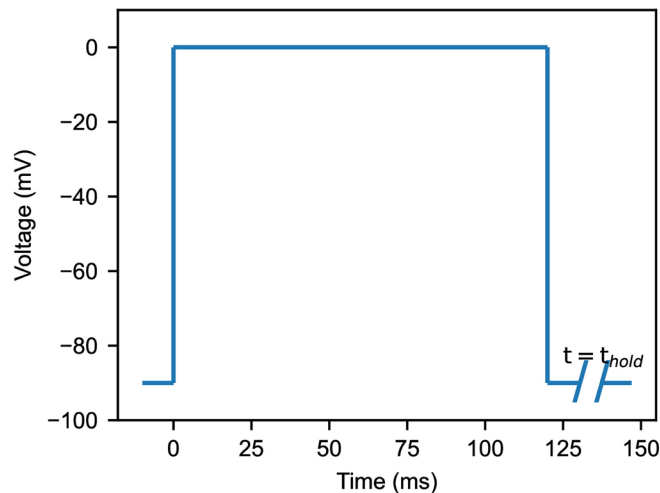


Figure 3. Voltage-clamp protocol used in the study with a holding potential duration of t_{hold} between two sweeps. t_{hold} was set to 10 , 20 , or 40 s depending upon the experiment.

area remains consistent with the hypothesised spherical surface area, allowing for accurate modelling of molecular interactions and local concentrations.

On the other hand, experimental parameters are difficult to control and are expected to vary from cell to cell. These include the channel permeability (\bar{P}_{Ca}), cell size (R_o), and time allowed for diffusion prior to the clamp being applied (t_o). Note that although experimenters can set the maximum and minimum possible value of t_o , the exact value cannot be controlled. We used the model to determine how variations in these three variables influence RCDI. We determine their range from our previous patch-clamp experiments as explained below.

Channel permeability (\bar{P}_{Ca}): The peak I_{CaL} value during a step to 0mV varied from -490.7 pA to -4444.4 pA in our experiments (see the online extended data). At the same time, for the I_{CaL} model defined in “Model of the L-type calcium current”, the peak value of the quantity ($O \times \delta_{GHK}$) during the step to 0mV was found to be -99917.3 C/m³ (also shown in online extended data). Therefore, \bar{P}_{Ca} was varied from 0.005 nL/s to 0.0444 nL/s ($\bar{P}_{Ca} = I/(O \times \delta_{GHK})$), and we used a default value of 0.04 nL/s for simulations in this study unless mentioned otherwise.

Cell size (R_o): The size of the cells used for the patch-clamp experiments was not measured individually for each cell. Therefore, we estimated the cell’s radius R_o by extrapolating the capacitive recordings and the microscopic measurement of the cell size made before the cells were cloned with Ca_v1.2. Using this method, R_o was found to vary from 2.5 μ m to 30 μ m for the experiments performed previously. Refer to the supplementary online data for a comprehensive breakdown detailing the methodology employed in this estimation.

Time given to the buffer to equilibrate into the cell (t_o): Some cells can rupture spontaneously to form whole-cell configuration thus allowing the intracellular solution to enter into the cell as soon as they are put on a chip plate¹⁷, while most others only do so when suction is applied to the cells. In our previous experiments, the time between placing cells on the plate and the onset of experiments was 5 minutes, while the time between the application of suction and the onset of experiments was 5 seconds.

In this study we also show that RCDI is governed by three time constants — t_o , t_{hold} , and t_{diff} , where t_{diff} is a function of R_o indicating the time the buffer will take for complete equilibration into the cell. To determine the range of t_{diff} we used an analytical solution for the diffusion of buffer in this geometry and configuration in the absence of Ca²⁺⁹. The analytical solution was used to calculate the t_{diff} required to achieve near-complete equilibration ($\sim 99.9\%$ of the maximum buffer concentration in the cell surface) and was found to be well approximated by a cubic function of R_o (see online extended data):

$$t_{diff} = 0.0163R_o^3 - 0.019R_o^2 + 0.008R_o - 0.016. \quad (9)$$

This equation was used to determine the range of t_{diff} which was found to vary from 144 ms to 423 s, corresponding to R_o varying from 2.5 μ m to 30 μ m, respectively. The permissible values of the timescales as per the experimental setup are depicted on a number line shown in Figure 4. The values of all parameters used for the model are given in Table 1.

Simulation of the model

Having established all the elements that comprise the RCDI model in the sections above, here we describe the numerical methods used for simulations.

Equation (2)–Equation (4) were discretised by adopting the finite volume method¹⁸ and dividing the hemispherical cell of radius R_o into N shells as shown in Figure 5. The diffusion terms were then written as a difference in flux using Fick’s first law of diffusion; this reduced the equations from second-order PDEs to a set of first-order

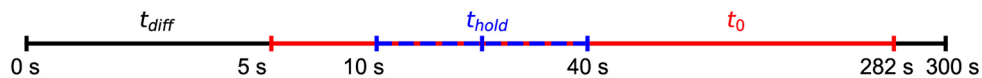


Figure 4. The range of values possible for 1) time required for equilibration of the free buffer into the cell (t_{diff}), 2) initial time before the experimental voltage clamp and recordings begin (t_o), and 3) time between successive voltage pulses (t_{hold}). While t_{diff} and t_o can take continuous values, t_{hold} can only take discrete value $\in \{10, 20, 40\}$ s.

Table 1. Parameters used as input for the model to predict RCDI. Parameters for which the exact value may vary across a range, the default value used is listed while the range is shown in brackets.

Parameter	Value
a_K	5×10^{-419}
a_{Na}	2.78×10^{-519}
K_{IC50}	0.9×10^{-6} mM
D_{Ca}	4×10^{-9} cm ² /ms ^{20,21}
D_B	2×10^{-9} cm ² /ms ²²
k_{off} at 310 [K]	0.298 ms ⁻¹²³
k_{on} at 310 [K]	1700 mM ⁻¹ ms ⁻¹²³
B_{max}	10 mM
R_h	$\frac{1}{\sqrt{2}}$ μm
R_0	30 μm (2 μm, 40.6 μm)
t_0	180 s (5 s, 300 s)
\bar{P}_{Ca}	0.04 nL/s (0.005 nL/s, 0.046 nL/s)

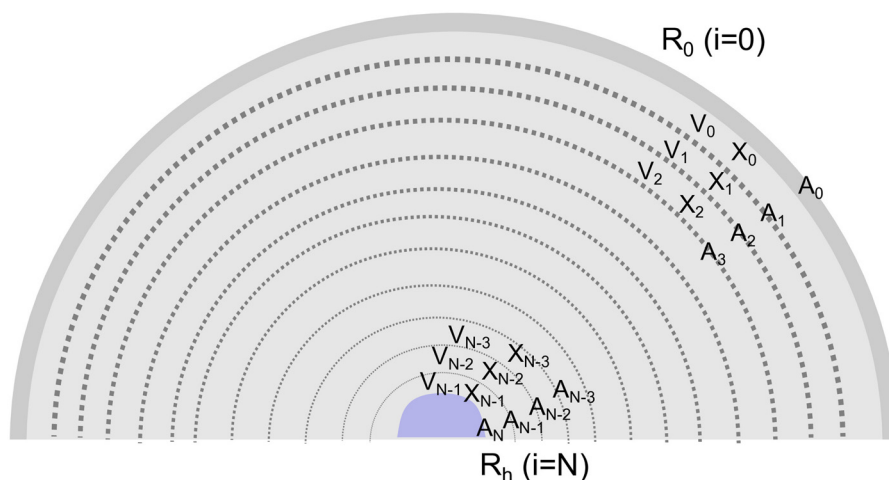


Figure 5. Schematic showing discretisation of the hemispherical cell into N shells.

ODEs. The chemical species within each discretised shell ($i = 1$ to $N - 1$) were computed simultaneously using a system of equations of the form:

$$\frac{d[X]_i}{dt} = D_X \frac{\overbrace{A_i([X]_{i-1} - [X]_i)}^{\text{flux across outer boundary}}}{LV_i} - D_X \frac{\overbrace{A_{i+1}([X]_i - [X]_{i+1})}^{\text{flux across inner boundary}}}{LV_i} \pm \overbrace{(k_{on} \cdot [Ca^{2+}]_i [B]_i - k_{off} \cdot [CaB]_i)}^{\text{chemical reaction}}, \quad (10)$$

where X represents the chemical species: Ca^{2+} , B, or CaB. Here, $L = (R_0 - R_h)/N$, $V_i = \frac{2}{3}\pi((R_0 - i \cdot L)^3 - (R_0 - (i + 1) \cdot L)^3)$, and A_i was calculated at each boundary as $2\pi(R_0 - i \cdot L)^2$. At the $i = 0$ boundary (in the outermost shell), there is no flux for [B] and [CaB], however, there is a voltage- and time-dependent flux of $[\text{Ca}^{2+}]$ given by $-I_{\text{CaL}}/(2FV_0)$. The constant values of the species at the inner shell boundary ($[X]_N$) along with the initial conditions are outlined in Equation (5) at $r = R_h$ and $t = 0$ respectively.

The above system of discretised equations was simulated using Myokit version 1.35.3²⁴, which incorporates the adaptive-timestep CVODES as the ODE solver, and both absolute and relative tolerances were set to 10^{-9} . The system was discretised such that the shell width (L) was $\approx 0.05 \mu\text{m}$ (see online extended data for convergence tests that show that the shell width should be $\approx 0.05 \mu\text{m}$ or lower to ensure negligible error in the simulations). For the largest possible cell with a radius of $30 \mu\text{m}$, N should be at least 572, to ensure $L \approx 0.05 \mu\text{m}$.

The RCDI shown in Figure 6 (bottom right) was simulated at $R_0 = 30 \mu\text{m}$, $t_0 = 180 \text{ s}$, and $t_{\text{hold}} = 10 \text{ s}$. On applying the voltage protocol, Ca^{2+} enters the cell via I_{CaL} . Although this Ca^{2+} is subject to diffusion and buffering as previously explained, some amount of calcium accumulates with time in the outermost shell (near the LCCs) in subsequent sweeps as shown in Figure 6 (top left). The increase in $[\text{Ca}^{2+}]_s$ per sweep relative to the first sweep is responsible for the decrease in the magnitude of the CDI gate of I_{CaL} , f_{Ca} in each sweep (Figure 6, top right). This in turn attenuates the magnitude of the source of Ca^{2+} itself — I_{CaL} (Figure 6, bottom left), thus leading to RCDI of the current. The peak I_{CaL} at each sweep is plotted in Figure 6 (bottom right), and is used to calculate rundown at any sweep i using peak I_{CaL} during the sweep ($|I_{\text{CaL}}^i|_{\text{max}}$) relative to the same quantity in sweep 1: $R_i = 1 - |I_{\text{CaL}}^i|_{\text{max}} / |I_{\text{CaL}}^1|_{\text{max}}$. The resultant rundown in this instance shows a saturating shape of the rundown-versus-time curve. The model was used to explore the qualitative impact of different experimental variables on RCDI.

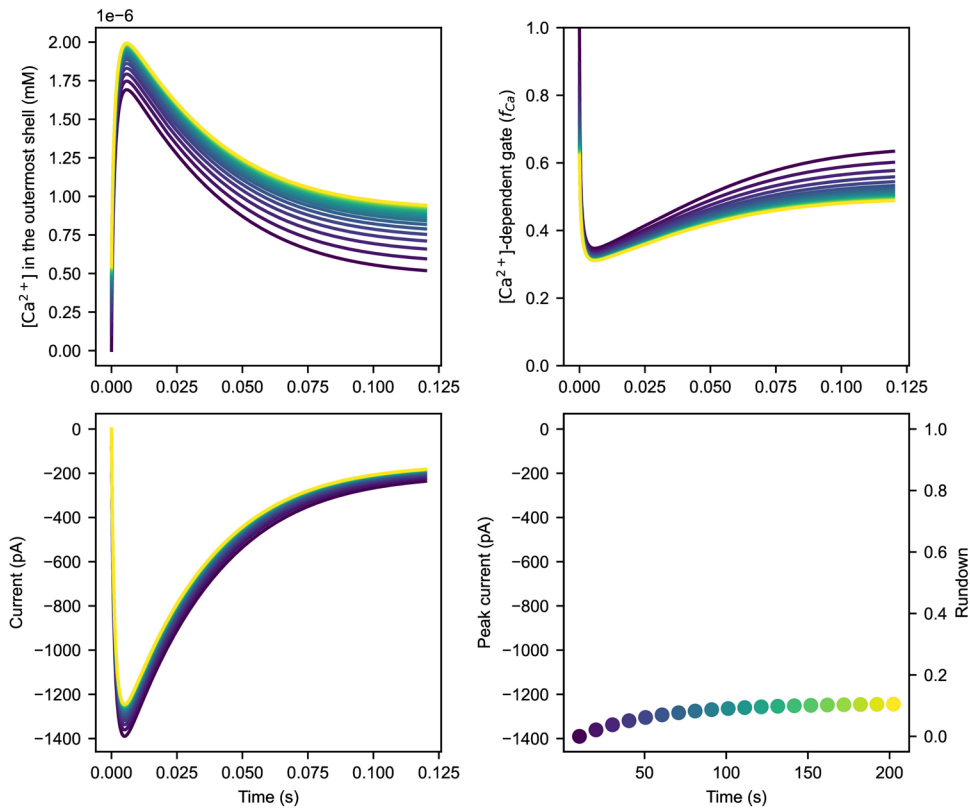


Figure 6. Top left: Simulation of the local $[\text{Ca}^{2+}]$ in the outermost shell (near the LCCs), Top right: Simulation of the CDI gate (f_{Ca}), and Bottom left: Simulation of I_{CaL} during the V_m step to 0 mV for successive sweeps with indigo and yellow corresponding to the first and last sweep respectively. Bottom right: Peak I_{CaL} simulated at each sweep against the sweep number. Simulation was done at $R_0 = 30 \mu\text{m}$, $t_0 = 180 \text{ s}$, and default values of t_{hold} , \bar{P}_{Ca} and B_{max} given in Table 1.

Results

Impact of experimental variables on RCDI

In this section, we show how variations in the experimental parameters — current permeability (\bar{P}_{Ca}), cell's radius (R_0), and diffusion interval before the application of the voltage-clamp (t_0) affect the concentration of free calcium and buffer near the LCCs. Change in \bar{P}_{Ca} is expected to drive CDI due to changes in the Ca^{2+} brought into the cell by I_{CaL} . For cells with the same \bar{P}_{Ca} but different sizes, those of the larger size are expected to undergo less CDI because of decrease in LCC density. Similarly, an increase in t_0 is expected to reduce CDI due to an increase in the availability of free buffer, which can interact with the available Ca^{2+} .

Here each experimental variable was individually set to its extreme permissible value resulting in eight unique parameter sets for the model (2³), representative of eight different cells. The model for each scenario was then simulated to the voltage as per the protocol described in 'voltage-clamp protocol' (with $t_{hold} = 10$ s).

Figure 7 shows the simulation of $[Ca^{2+}]_s$ and free buffer in the outermost shell ($[B]_s$) for each of the eight 'model' cells. Within each plot, the submembrane Ca^{2+}/B concentration transients simulated during the channel opening steps of successive sweeps are plotted next to each other. The *change* in magnitude of the peak Ca^{2+}/B per sweep is indicative of RCDI, and the *rate of change* of RCDI forms the shape of the rundown-versus-time curve.

Figure 7 shows that change in the magnitude of peak Ca^{2+}/B across sweeps reflective of RCDI only occurs for large cells (see the bottom two rows of Figure 7). Even though an increase in cell size leads to a decrease in CDI (compare subplots A with E and C with G), the smallest cell does not undergo RCDI, while the largest cell does. This can be explained by the lack of complete buffer replenishment in the bigger cells over the course of the experiment as they require more time for equilibration of buffer into the cell (t_{diff}) than smaller cells.

For large cells in which RCDI occurs, change in \bar{P}_{Ca} impacts the extent of RCDI. Comparison of subplot G with H shows an increase in CDI (evident from the higher $[Ca^{2+}]_s$), as well as an increase in RCDI (evident from the greater percentage increase in $[Ca^{2+}]_s$ in subplot H compared to G). This is further illustrated by the simulations shown in Figure 8 (at default R_0 and t_0), where there is an increase in the magnitude of RCDI for higher \bar{P}_{Ca} values—both saturating and inverse.

Similarly, for large cells in which RCDI occurs, change in t_0 impacts the shape of RCDI against time. Figure 7E and F show that when t_0 is small, $[B]_s$ increases many fold over the course of the experiment, regardless of the LCC current density. Peak $[Ca^{2+}]_s$ correspondingly decreases per sweep, as incoming Ca^{2+} immediately reacts with the buffer through time, before saturating when the buffer concentration is high enough. This would translate to less CDI per sweep and increased LCC currents — an inverse RCDI against time (see the online supplement at <https://github.com/CardiacModelling/L-type-Ca-rundown-modelling/blob/main/ExtendedData.ipynb>).

On the other hand, in Figure 7G and H we see that when t_0 is large, the additional time before the experiment allows the free buffer to equilibrate into the cell before the voltage-clamp is applied, thus reducing CDI for the first sweep compared to a similar cell with smaller t_0 . Peak $[Ca^{2+}]_s$ increases per sweep before saturating which would translate to increasing CDI per sweep, lower I_{CaL} , and more RCDI over time which eventually stabilises — saturating rundown against time (See the online supplement at <https://github.com/CardiacModelling/L-type-Ca-rundown-modelling/blob/main/ExtendedData.ipynb>). The accumulation of $[B]_s$ increases per sweep here as well for smaller t_0 , but the proportion of increase is much smaller, and the rate of reaction of calcium with buffer is limiting and it allows $[Ca^{2+}]_s$ to build up over time.

In this section, we showed that the cell size determines *whether* RCDI will occur or not, \bar{P}_{Ca} affects the extent of RCDI, and t_0 influences the shape of the rundown-versus-time curve. Further, of the three types of rundown patterns identified in the previous study, two of them—saturating and inverse patterns—were found to be explained by the change in CDI predicted by the model of this study.

Impact of inter-pulse diffusion time on RCDI

In the previous section, we observed that the lack of complete buffer equilibration into the cell gives rise to RCDI. In this section, we additionally investigate how the time give to the buffer to diffuse in *between* each sweep affects RCDI. This was done by repeating identical simulations at three different t_{hold} (10, 20, and 40 s).

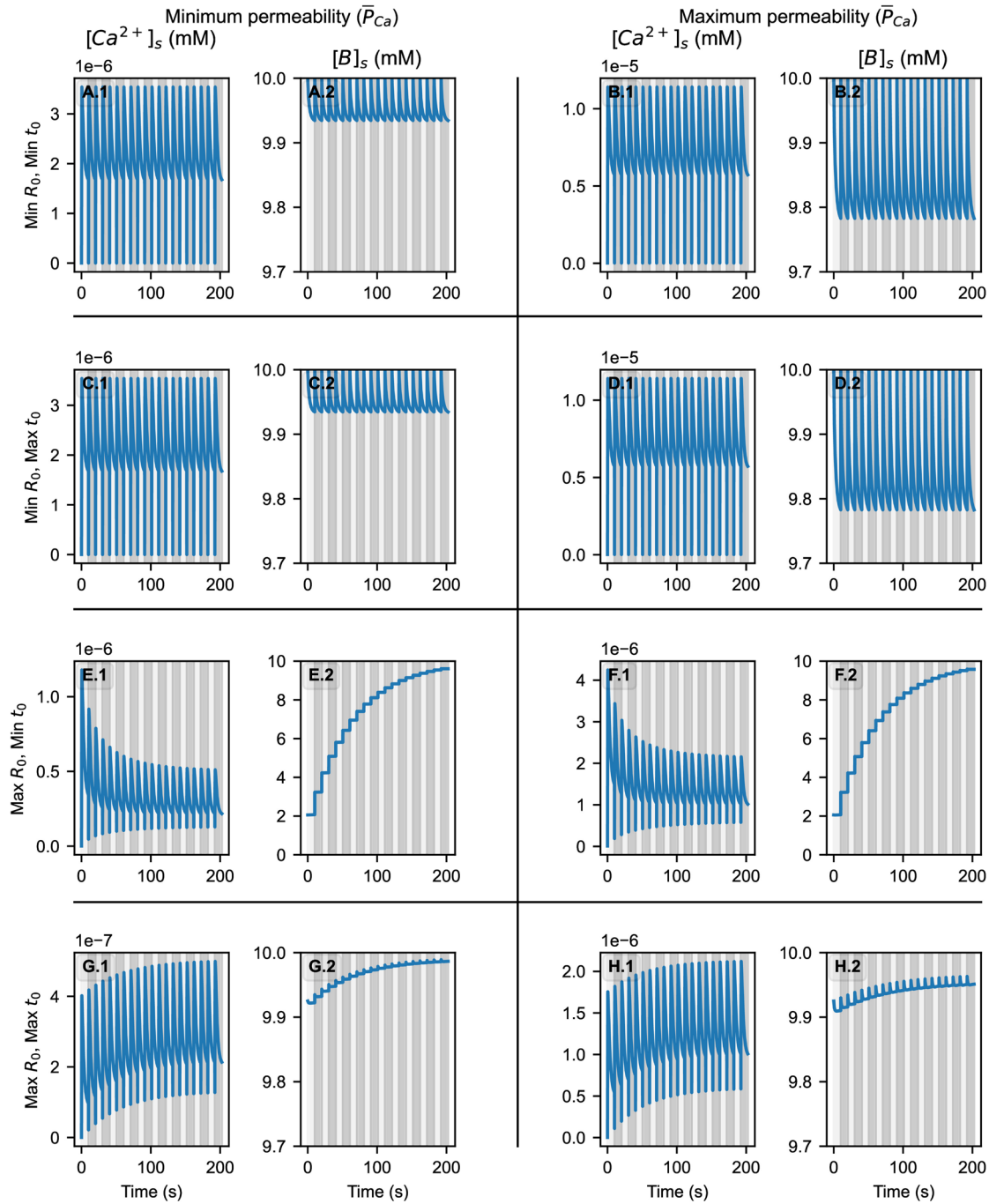


Figure 7. The effect of different experimental parameter extremes on submembrane calcium and free buffer concentrations. Concentrations are plotted from simulation results in the outermost shell (near the LCCs) during the channel opening steps to 0 mV, and are plotted successively with alternating grey backgrounds highlighting alternating sweeps. These simulations were performed for eight unique conditions spanning over the corner cases of \bar{P}_{Ca} , t_{off} and R_0 , while t_{hold} and B_{max} were kept at default values as shown in Table 1.

At each t_{hold} the model was simulated as per the protocol for 20 sweeps at ten different values of t_0 varying from 10 s to 300 s, while P_{Ca} and R_0 were kept at default values. The resultant rundown simulated is shown in Figure 9, for t_{hold} equal to 10 s (left), 20 s (centre), and 40 s (right).

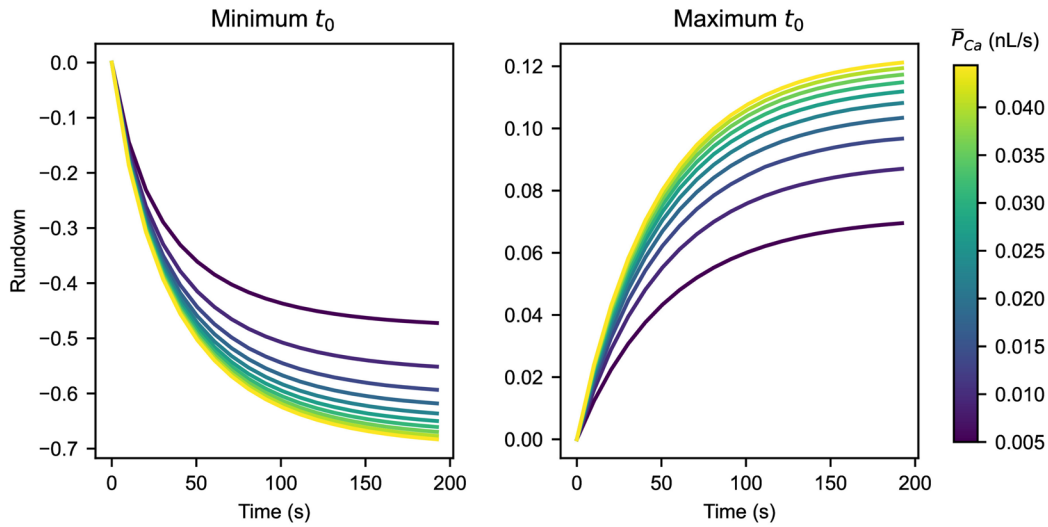


Figure 8. Simulation of rundown for the largest possible cells ($R_0 = 30 \mu\text{m}$) with different \bar{P}_{Ca} per cell varied across its permissible range at the minimum t_0 (Left) and maximum t_0 (Right). B_{max} and t_{hold} were kept at default values shown in Table 1.

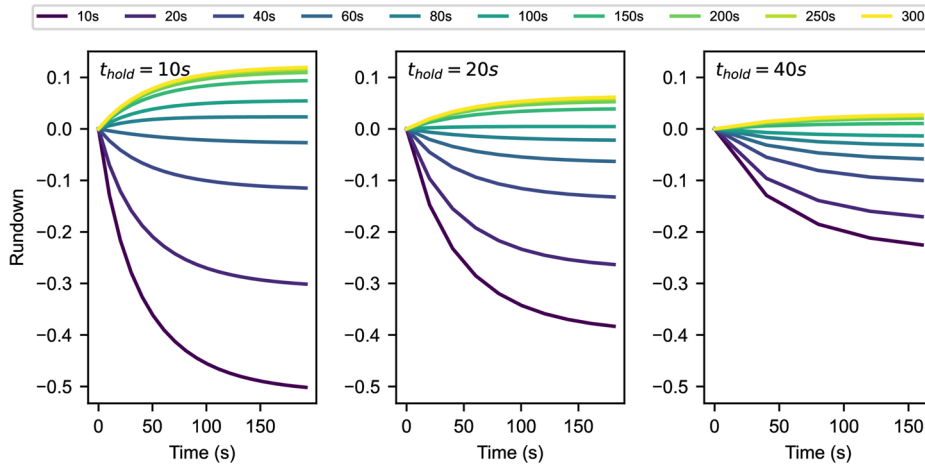


Figure 9. Rundown for the largest possible cells ($R_0 = 30 \mu\text{m}$), with each cell at different t_0 and t_{hold} of 10 s (Left), 20 s (Centre), and 40 s (Right). \bar{P}_{Ca} and B_{max} were kept at default values.

All three subplots show that at very small t_0 , the rundown-versus-time pattern is ‘inverse’, while at bigger t_0 this trend becomes saturating. This is consistent with the observation of change in pattern of RCDI from inverse to saturating rundown on increasing t_0 in Figure 7 (E to G and F to H). Figure 9 shows a decrease in the number of saturating RCDI trends with increasing t_{hold} as well as an increase in the number of inverse RCDI trends. The longer time between each sweep allows more buffer to be replenished than at smaller t_{hold} , thus explaining the change in trend.

In this section, we showed that for large cells in which RCDI occurs, t_{hold} and t_0 together determine the shape of the rundown-versus-time curve — inverse or saturating.

Time constants relationship governing RCDI

In this section, we show that whether RCDI will form a saturating or an inverse pattern with time can be predicted based on the values taken up by three time constants — t_{diff} , t_0 , or t_{hold} . The shape of the rundown pattern depends on a complex interaction of the three time scales given by ζ , which was determined heuristically to be:

$$\zeta = \frac{t_0^2}{t_{diff} t_{hold}}. \quad (11)$$

If ζ is greater than 1.5, then the resulting rundown pattern is predicted to be saturating while if it is less than 1.5, then it is predicted to be inverse. Between 1.5 and 4.5, the pattern can be either inverse ($P = 20\%$) or saturating ($P = 0\%$) as shown in the online extended data.

The predictive capabilities of ζ are illustrated in Figure 10, wherein we independently simulated and plotted RCDI for three distinct scenarios. In the first scenario, t_{diff} represents the smallest time constant (left), in the second scenario, t_0 is the smallest time constant (centre), and in the third scenario, t_{hold} is the smallest. For each scenario, ten examples are presented, and model parameters are chosen by randomly selecting time constants from their permissible range, as depicted on the number line in Figure 4, while B_{max} and \bar{P}_{Ca} are maintained at their default values. The resulting rundown per draw was simulated across twenty sweeps for ten draws per scenario.

Further, Figure 10 (left) confirms the absence of RCDI in very small cells since it shows minimal rundown when t_{diff} is the smallest time constant, aligning with the characteristics observed in the first two rows of Figure 7. Additionally, when t_0 is the smallest constant, then $\zeta < 1$, which should almost always lead to an inverse RCDI. This is also confirmed by the centre panel of Figure 10. ζ is most useful to predict the RCDI pattern when t_{hold} is the smallest time constant, where it accurately predicts the outcome with 99.8% accuracy (see the online data for details).

In this section, we showed that the relationship amongst the timescales determines whether RCDI occurs, and if applicable, the shape of that rundown against time using ζ . The relationship represented by ζ was validated by our model.

Impact of maximum buffer concentration on rundown

So far we have seen that RCDI can be attributed to the change in the availability of the buffer near the LCCs per sweep. We have shown that within the experimental setup we previously adopted in Agrawal *et al.*⁷, large cells are susceptible to RCDI because the buffer does not fully equilibrate into these cells due to limits of t_0 and t_{hold} . In this section, we validate the role of buffer supply (diffusion) in RCDI, by exploring the impact of hypothetical experimental setups at different B_{max} on RCDI.

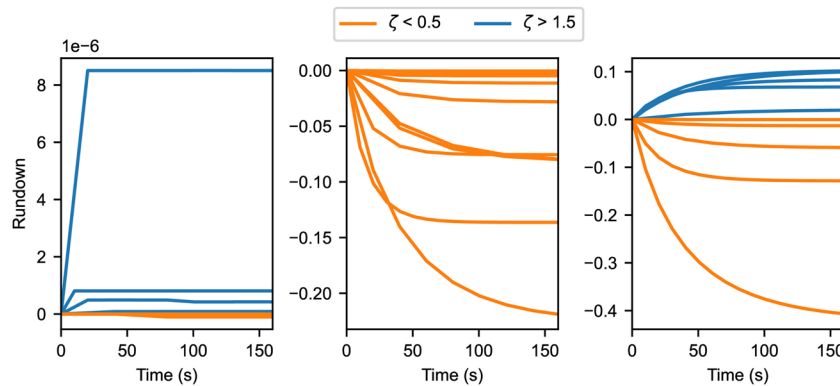


Figure 10. Rundown simulated for cells where R_0 , t_0 , and t_{hold} are determined by the random draw of the time constants from the number line shown in Figure 4. The random draw is performed ten times each such that the minimum time constant is t_{diff} (Left), t_0 (Centre), and t_{hold} (Right). \bar{P}_{Ca} and B_{max} are kept at default values given in Table 1 and the value of ζ is given by Equation 11.

We know that higher accumulation of Ca^{2+} per sweep will lead to more usage of buffer. By reducing the maximum available buffer (B_{max}), the accumulation of Ca^{2+} increases, which in turn increases the usage of buffer per sweep. Previous observations indicated that, within our established experimental conditions, large cells exhibited maximum signs of RCDI. We hypothesise that modifying B_{max} might alter this behaviour, providing a fresh perspective on ways to minimise RCDI in experiments.

To test this hypothesis, we explored conditions at which RCDI can be minimised in the largest possible cell ($R_0 = 30 \mu\text{m}$). We chose time constants that allow for maximum equilibration of buffer into the cell such as $t_0 = 300 \text{ s}$ and $t_{\text{hold}} = 10 \text{ s}$. **Figure 11** (left) shows the current simulated in the first sweep at different B_{max} while the right panel shows the corresponding RCDI. The simulation at the default $B_{\text{max}} = 10 \text{ mM}$ is highlighted in red. This figure shows that CDI decreases with an increase in B_{max} , while RCDI decreases switching from a saturating to an inverse trend.

Figure 12 extends this analysis to smaller cells ($R_0 = 10, 15, \text{ and } 20 \mu\text{m}$), emphasising that considerable saturating rundown can be induced in smaller cells at reduced B_{max} . While the simulation at the default $B_{\text{max}} = 10 \text{ mM}$ (red plot in **Figure 12**, right) yielded negligible RCDI, a decrease in B_{max} results in a substantial increase in the rundown, deteriorating to as much as 60% of the initial current. While this figure shows that RCDI can be induced for smaller cells by changing B_{max} , it also shows that smaller cells remain less susceptible to RCDI as the affect of change in B_{max} is higher on larger cells (right panel), than on smaller cells (left panel).

This section shows that changes in B_{max} have an impact on RCDI for cells of all sizes, while larger cells nevertheless continue to show a more pronounced RCDI than smaller cells. This finding is aligned with the emergent conclusion from the previous results that buffer dynamics plays a crucial role in influencing RCDI.

Discussion

Current recordings of patch-clamp experiments from isolated L-type calcium channels (LCCs) are known to be contaminated with rundown. Previous studies have attributed this phenomenon to various factors, including washing away of phosphorylating agents (e.g. ATP), loss of LCC channels over time, and increased accumulation of intracellular Ca^{2+} ^{3,4,6}. Our prior experimental work⁷ associated increased rundown with the accumulation of intracellular $[\text{Ca}^{2+}]$ and, by extension, calcium-dependent inactivation (CDI). This earlier study showed that while the quantitative rundown of I_{CaL} varies from cell to cell, qualitatively, this rundown takes three predominant shapes against time — linear, saturating, and inverse (where I_{CaL} 's magnitude increases rather than decreases with time). In this study, we extend our understanding by employing a model that replicates experimental conditions of patch-clamp experiments adopted previously⁷. By simulating Ca^{2+} entry, its chemical reaction with buffer B to form the complex CaB, and subsequent diffusion, we aim to

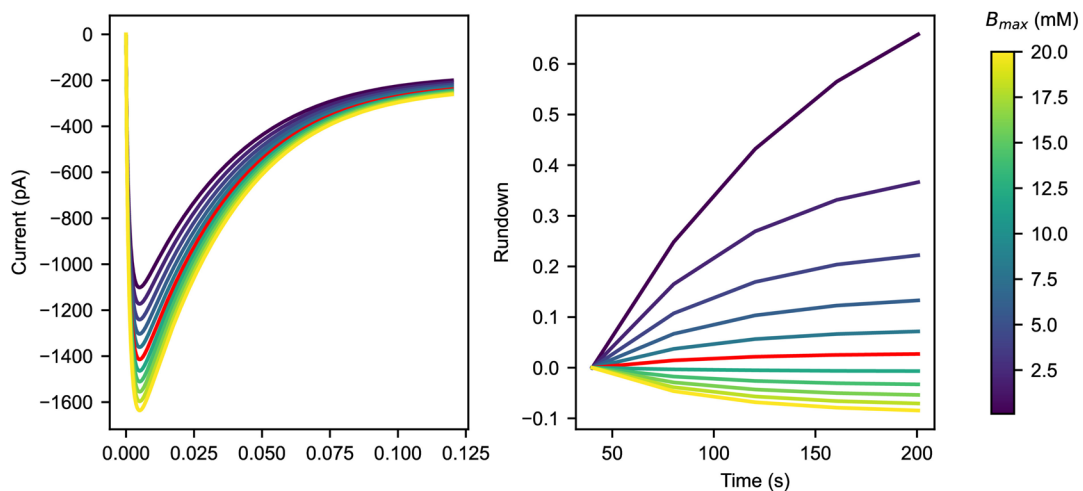


Figure 11. Left: Current simulated in the first sweep for cell with $R_0 = 30 \mu\text{m}$, $t_0 = 300 \text{ s}$, $t_{\text{hold}} = 10 \text{ s}$ and ten distinct B_{max} . Right: Corresponding rundown simulated for each B_{max} . Simulations at $B_{\text{max}} = 10 \text{ mM}$ are highlighted in red.

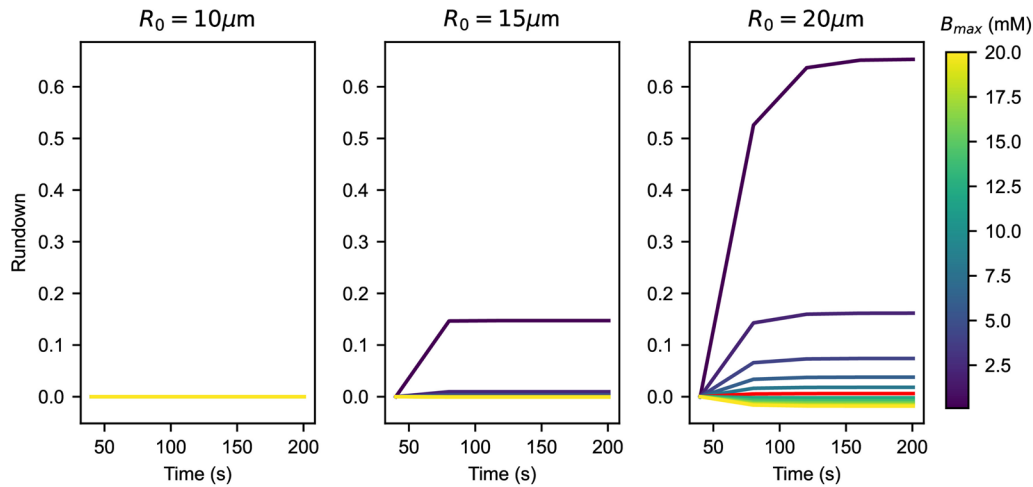


Figure 12. Rundown simulated at $R_0 = 10 \mu\text{m}$ (left), $15 \mu\text{m}$ (centre), and $20 \mu\text{m}$ (right). Simulations were performed at $t_0 = 300 \text{ s}$, $t_{\text{hold}} = 10 \text{ s}$ and ten distinct B_{max} .

determine if rundown due to CDI (RCDI) can qualitatively explain the observed experimental rundown patterns. Additionally, we use the model to determine the impact of choice of user-defined (t_{hold} and B_{max}) and experimental parameters (\bar{P}_{Ca} , R_0 , and t_0) on RCDI.

Our model successfully reproduced two qualitative rundown patterns, namely “saturating” and “inverse”, mirroring experimental observations. Notably, the “linear” rundown shape remained elusive in our simulations, suggesting that RCDI dominantly contributes to “saturating” and “inverse” patterns only. RCDI’s development was found to be governed by the restrictions in the supply of buffer near the LCCs both before and during voltage opening steps. Figure 7 demonstrates that RCDI primarily affects large cells under our base experimental conditions⁷ ($B_{\text{max}} = 10 \text{ mM}$), but not the smaller cells. Further, for large enough cells in which RCDI occurs, increase in incoming Ca^{2+} was found to be associated with increased RCDI (Figure 8), in agreement with findings from Agrawal *et al.*⁷ that conditions which promote higher accumulation of Ca^{2+} will have more rundown. Since noticeable RCDI only occurs for large cells ($R_0 > 20 \mu\text{m}$) and not for the average-sized CHO cell transfected with $\text{Ca}_v1.2$ ($R_0 = 10 \mu\text{m}$), RCDI is likely not a major factor contributing towards rundown. Indeed, our previous study showed that experimental conditions that promote accumulation of Ca^{2+} only account for 40% of rundown⁷.

The study highlights the significant impact of buffer dynamics on RCDI. RCDI was observed to be influenced by constraints in the supply of buffer near the LCCs, both before and during voltage opening steps. This is further confirmed by changes in B_{max} affecting RCDI for cells of all sizes. The decrease in B_{max} correlates with increased accumulation of Ca^{2+} per sweep, leading to enhanced saturating rundown. Conversely, very high B_{max} leads to inverse pattern of RCDI, not driven by small t_0 like in Figure 7 and Figure 9, rather because the reduction in requirement of buffer per sweep allows a net reduction in accumulation of Ca^{2+} .

In this study, we accounted for the variations in ‘real-world’ experimental conditions such as t_0 , R_0 , and \bar{P}_{Ca} which are challenging to standardise across all experiments. Unsurprisingly, variations in these input variables resulted in variations in the predicted RCDI as well. In view of this variability, it is important to consider that cell-to-cell variability in recorded current or *extrinsic variability*²⁵, may also be rooted in variability in the individual cell’s experimental conditions and not just morphological differences.

This study is the first, to our knowledge, to model rundown due to CDI (RCDI). In future investigations, measuring rundown in these cells should include an assessment of cell size to facilitate the development of cell-specific models for RCDI. This approach can enable the quantitative evaluation of CDI’s contribution to rundown, extending beyond the qualitative analysis conducted in this study.

In terms of experimental design and takeaways, future studies should allow sufficient time for buffer diffusion into the cell by extending the interval between ‘application of suction’ and voltage clamping to 5 minutes, thus increasing t_o . Additionally, efforts should be made to maintain a high replenishment time between sweeps (high t_{hold}), although this may be challenging due to experiment duration constraints. While completely eliminating RCDI is challenging due to the transient nature of the rundown-versus-time pattern (switching from saturating to inverse with increased buffer availability, as shown in [Figure 11–Figure 12](#)), the use of small cells and high B_{max} can contribute to reducing RCDI.

Conclusions

Our computational model successfully replicated experimental conditions, providing insights into rundown of L-type calcium current (I_{CaL}). Rundown due to CDI (RCDI) qualitatively explained the saturating and inverse rundown patterns observed in large cells. The underlying mechanism of RCDI was found to be the buffer kinetics near the LCCs, determined by user-defined experimental conditions such as the equilibration time of buffer before (t_o) and during voltage-clamping (t_{hold}), and the buffer concentration in the intracellular solution (B_{max}). Current permeability was also found to influence this dynamics, but it is challenging to control or screen out. This study highlights the importance of considering cell-specific conditions in data interpretation. Future work should optimise the time allowed for buffer to equilibrate before the recordings begin (t_o) and the inter-pulse interval in the voltage clamp protocol (t_{hold}) to facilitate buffer equilibration into the cell. The use of small cells and high B_{max} can further mitigate rundown contamination of I_{CaL} recordings.

Ethics and consent

Ethical approval and consent were not required.

Data and software availability

All code and supporting material available from: <https://github.com/CardiacModelling/L-type-Ca-rundown-modelling>.

Archived code and supporting material at time of publication: <https://doi.org/10.5281/zenodo.14186292>²⁶.

License: The code is available under the terms of The BSD 3-clause licence.

Data are available under the terms of the Creative Commons Attribution 4.0 International license (CC-BY 4.0).

Acknowledgements

The authors thank Michael Colman and Denis Noble for their feedback based on careful reading of an earlier draft of this work as part of A.A.’s Doctorate of Philosophy thesis.

References

- Hofmann F, Flockerzi V, Kahl S, *et al.*: **L-type $Ca_v1.2$ calcium channels: from *in vitro* findings to *in vivo* function.** *Physiol Rev.* 2014; **94**(1): 303–326.
[PubMed Abstract](#) | [Publisher Full Text](#)
- Molleman A: **Patch clamping: an introductory guide to patch clamp electrophysiology.** John Wiley & Sons, 2003.
[Publisher Full Text](#)
- Belles B, Malecot CO, Hescheler J, *et al.*: **“Run-down” of the Ca current during long whole-cell recordings in guinea pig heart cells: role of phosphorylation and intracellular calcium.** *Pflugers Arch.* 1988; **411**(4): 353–360.
[PubMed Abstract](#) | [Publisher Full Text](#)
- Sarantopoulos C, McCallum JB, Kwok WM, *et al.*: **β -escin diminishes voltage-gated calcium current rundown in perforated patch-clamp recordings from rat primary afferent neurons.** *J Neurosci Methods.* 2004; **139**(1): 61–68.
[PubMed Abstract](#) | [Publisher Full Text](#)
- Kameyama M, Kameyama A, Kaibara M, *et al.*: **Intracellular mechanisms involved in “run-down” of calcium channels.** In: *Calcium Protein Signaling.* Springer, 1989; 111–117.
[Publisher Full Text](#)
- McNaughton NC, Bleakman D, Randall AD: **Electrophysiological characterisation of the human N-type Ca^{2+} channel II: activation and inactivation by physiological patterns of activity.** *Neuropharmacology.* 1998; **37**(1): 67–81.
[PubMed Abstract](#) | [Publisher Full Text](#)
- Agrawal A, Clerx M, Wang K, *et al.*: **An experimental investigation of rundown of the l-type calcium current [version 1; peer review: 2 approved with reservations, 1 not approved].** *Wellcome Open Res.* 2024; **9**: 250.
[Publisher Full Text](#)
- Agrawal A, Clerx M, Wang K, *et al.*: **Modelling the effect of intracellular calcium in the rundown of l-type calcium current.** In: *2022 Computing in Cardiology (CinC).* IEEE, 2022; **498**: 1–4.
[Publisher Full Text](#)
- Agrawal A, Wang K, Polonchuk L, *et al.*: **Models of the cardiac L-type calcium current: a quantitative review.** *WIREs Mech Dis.* 2023; **15**(1): e1581.
[PubMed Abstract](#) | [Publisher Full Text](#) | [Free Full Text](#)
- Hemond HF, Fechner EJ: **Chemical fate and transport in the environment.** Elsevier, 2014.
[Reference Source](#)

11. Zeng J, Laurita KR, Rosenbaum DS, *et al.*: **Two components of the delayed rectifier K⁺ current in ventricular myocytes of the guinea pig type: theoretical formulation and their role in repolarization.** *Circ Res.* 1995; **77**(1): 140–152.
[PubMed Abstract](#) | [Publisher Full Text](#)
12. Kubalova Z: **Inactivation of L-type calcium channels in cardiomyocytes. Experimental and theoretical approaches.** *Gen Physiol Biophys.* 2003; **22**(4): 441–454.
[PubMed Abstract](#)
13. Sham JS, Cleemann L, Morad M: **Functional coupling of Ca²⁺ channels and ryanodine receptors in cardiac myocytes.** *Proc Natl Acad Sci U S A.* 1995; **92**(1): 121–125.
[PubMed Abstract](#) | [Publisher Full Text](#) | [Free Full Text](#)
14. Stotz SC, Jarvis SE, Zamponi GW: **Functional roles of cytoplasmic loops and pore lining transmembrane helices in the voltage-dependent inactivation of HVA calcium channels.** *J Physiol.* 2004; **554**(Pt 2): 263–273.
[PubMed Abstract](#) | [Publisher Full Text](#) | [Free Full Text](#)
15. Hodgkin AL, Huxley AF: **A quantitative description of membrane current and its application to conduction and excitation in nerve.** *J Physiol.* 1952; **117**(4): 500–544.
[PubMed Abstract](#) | [Publisher Full Text](#) | [Free Full Text](#)
16. Davies CW, Malpass VE: **Ion association and the viscosity of dilute electrolyte solutions Part 1.—Aqueous inorganic salt solutions.** *Transactions of the Faraday Society.* 1964; **60**: 2075–2084.
[Publisher Full Text](#)
17. Py C, Martina M, Diaz-Quijada GA, *et al.*: **From understanding cellular function to novel drug discovery: the role of planar patch-clamp array chip technology.** *Front Pharmacol.* 2011; **2**: 51.
[PubMed Abstract](#) | [Publisher Full Text](#) | [Free Full Text](#)
18. Fallah NA, Bailey C, Cross M, *et al.*: **Comparison of finite element and finite volume methods application in geometrically nonlinear stress analysis.** *Appl Math Model.* 2000; **24**(7): 439–455.
[Publisher Full Text](#)
19. Shannon TR, Wang F, Puglisi J, *et al.*: **A mathematical treatment of integrated Ca dynamics within the ventricular myocyte.** *Biophys J.* 2004; **87**(5): 3351–3371.
[PubMed Abstract](#) | [Publisher Full Text](#) | [Free Full Text](#)
20. Wu YC, Tucker T, Fettiplace R: **A theoretical study of calcium microdomains in turtle hair cells.** *Biophys J.* 1996; **71**(5): 2256–2275.
[PubMed Abstract](#) | [Publisher Full Text](#) | [Free Full Text](#)
21. Kits KS, de Vlieger TA, Kooi BW, *et al.*: **Diffusion barriers limit the effect of mobile calcium buffers on exocytosis of large dense cored vesicles.** *Biophys J.* 1999; **76**(3): 1693–1705.
[PubMed Abstract](#) | [Publisher Full Text](#) | [Free Full Text](#)
22. Nowycky MC, Pinter MJ: **Time courses of calcium and calcium-bound buffers following calcium influx in a model cell.** *Biophys J.* 1993; **64**(1): 77–91.
[PubMed Abstract](#) | [Publisher Full Text](#) | [Free Full Text](#)
23. Lattanzio FA Jr, Bartschat DK: **The effect of pH on rate constants, ion selectivity and thermodynamic properties of fluorescent calcium and magnesium indicators.** *Biochem Biophys Res Commun.* 1991; **177**(1): 184–191.
[PubMed Abstract](#) | [Publisher Full Text](#)
24. Clerx M, Collins P, de Lange E, *et al.*: **Myokit: a simple interface to cardiac cellular electrophysiology.** *Prog Biophys Mol Biol.* 2016; **120**(1–3): 100–114.
[PubMed Abstract](#) | [Publisher Full Text](#)
25. Whittaker DG, Clerx M, Lei CL, *et al.*: **Calibration of ionic and cellular cardiac electrophysiology models.** *Wiley Interdiscip Rev Syst Biol Med.* 2020; **12**(4): e1482.
[PubMed Abstract](#) | [Publisher Full Text](#) | [Free Full Text](#)
26. Agrawal A, Mirams G: **L-type-ca-rundownmodelling: v1. 0.** 2024. <https://www.doi.org/10.5281/zenodo.14186293>